Original Article

MYO1B enhances colorectal cancer metastasis by promoting the F-actin rearrangement and focal adhesion assembly via RhoA/ROCK/FAK signaling

Lang Xie[1#], Hongyun Huang[1#], Zheng Zheng[1], Qian Yang[1], Shubo Wang[2], Yaoxu Chen[2], Jinlong Yu[1], Chunhui Cui[1]

[1]Department of General Surgery, Zhujiang Hospital, Southern Medical University, Guangzhou, China; [2]The Medical Department, 3D Medicines Inc., Shanghai, China

Contributions: (I) Conception and design: L Xie, J Yu, C Cui; (II) Administrative support: L Xie; (III) Provision of study materials or patients: H Huang, Z Zheng, Q Yang; (IV) Collection and assembly of data: H Huang, Z Zheng, S Wang, Y Chen, Q Yang; (V) Data analysis and interpretation: L Xie; (VI) Manuscript writing: All authors; (VII) Final approval of manuscript: All authors.

[#]These authors contributed equally to this work.

Correspondence to: Chunhui Cui; Jinlong Yu. Department of General Surgery, Zhujiang Hospital, Southern Medical University, Guangzhou, China. Email: drcuich@163.com; yujinlong640506@163.com.

Background: Colorectal cancer (CRC) has a high worldwide incidence and mortality. Tumor metastasis is one of the primary reasons for the poor prognosis of CRC patients. However, the mechanism underlying CRC metastasis is still unclear. Myosin 1B (MYO1B) is important for cell migration and motility and is part of the myosin superfamily that contains various myosins. Studies of prostate, cervical, and head and neck cancer have revealed preliminary findings concerning the effect of MYO1B on tumor metastasis. However, the role of MYO1B in CRC metastasis, as well as its underlying mechanism, remains unknown.

Methods: Quantitative real-time PCR and immunohistochemical staining methods were used to analyze the expression of MYO1B in human CRC and normal mucosa tissues. Lentivirus vector-based MYO1B oligonucleotides and short hairpin RNA (shRNA) were used to examine the functional relevance of MYO1B in CRC cells. Co-immunoprecipitation, western blotting, and immunofluorescence assays were used to investigate the underlying mechanism of MYO1B-mediated cell migration.

Results: The expression of MYO1B was increased in most CRC tissues and was positively associated with a greater risk of tumor metastasis and poor prognosis for patients. MYO1B was significantly associated with the migration and invasion properties of CRC cells *in vitro* and *in vivo*. MYO1B promoted F-actin rearrangement through the ROCK2/LIMK/Cofilin axis by enhancing the activation of RhoA. MYO1B also promoted the assembly of focal adhesions by targeting RhoA.

Conclusions: MYO1B plays a vital role in CRC metastasis by promoting the activation of RhoA. MYO1B may not only be a valid biomarker for predicting the risk of metastasis and poor prognosis in CRC but may also be a potential therapeutic target for patients with a high risk of tumor metastasis.

Keywords: Colorectal cancer (CRC); tumor metastasis; myosin 1B (MYO1B); cytoskeleton rearrangement; focal adhesion

Submitted Apr 13, 2021. Accepted for publication Oct 22, 2021.
doi: 10.21037/atm-21-4702
View this article at: https://dx.doi.org/10.21037/atm-21-4702

Introduction

Colorectal cancer (CRC) is the third most common type of cancer and the second leading cause of cancer-related death worldwide (1). Data from the Global Cancer Observatory (GCO) showed that more than 1.8 million patients were newly diagnosed with CRC in 2018, and there are approximately 0.88 million CRC-associated deaths each year (1). Many studies have demonstrated that tumor metastasis is the primary reason for the poor prognosis of CRC patients (2-6). However, due to the multitude of factors and processes associated with the incidence and progression of CRC, identifying the underlying mechanisms involved in CRC continues to be an extremely complex and challenging endeavor (7-10). There are many studies for mechanisms of CRC metastasis (11). Actin dynamics is involved in several biological processes, including metastasis of cancer cells in CRC, and it is thought to be associated with proteins such as FAK, Rho GTPases, PI3K, etc. (12). However, further studies in CRC are needed on its exact function and signal pathways involved. Our previous study screened potential target genes involved in CRC metastasis, including myosin 1B (MYO1B), which is an actin depolymerase (6). Due to its function, study of MYO1B may explain the underlying pathway and mechanism involved in regulation of Actin dynamics in CRC.

Myosins are a large and diverse superfamily of molecular motors that are important for cell migration and motility (13). Human myosins can be subdivided into 12 classes, among which class I myosins are the most conserved and widespread members (13,14). Aberrant overexpression of class I myosins not only drives cells toward a more migratory phenotype but also plays a vital role in regulating endocytosis, vesicle shedding, channel gating, and cell signaling (15-17). Growing evidence indicates that an increased expression of MYO1B plays a significant role in tumor metastasis in prostate (13), cervical (18), and head and neck cancers (19,20). However, its role in CRC metastasis is still unclear.

Actin filaments (F-actin) regulate cell morphology and movement by providing a variety of dynamic architectures (21). During the migration of cancer cells, actin networks continually undergo assembly and disassembly, mediated in space and time under the control of regulatory proteins (22). A recent study proved that MYO1B is an important depolymerase of actin (21), but its role and underlying mechanism in the F-actin rearrangement of CRC cells remains unknown.

Thus, the present study aims to investigate the role of MYO1B in CRC metastasis and achieve further insights into the mechanism of MYO1B-mediated cell migration and invasion.

We present the following article in accordance with the ARRIVE reporting checklist (available at https://dx.doi.org/10.21037/atm-21-4702).

Methods

Clinical samples

Fresh primary CRC samples with paired normal colorectal tissues (50 cases) were obtained from the Department of General Surgery in Zhujiang Hospital, Southern Medical University, Guangzhou, China, between 2012 and 2018. The distance between the cancerous and paired adjacent normal tissues was at least 2 cm. Paraffin samples (101 cases of tumor tissues from CRC patients and 77 cases of normal colorectal tissues from healthy people) were obtained from the Tissue Bank of Zhujiang Hospital between 2012 and 2018. The pathological diagnosis of each case was made by the Department of Pathology in Zhujiang Hospital. All procedures performed in this study involving human participants were in accordance with the Declaration of Helsinki (as revised in 2013). The study was approved by Ethics Committee of Zhujiang Hospital of Southern Medical University and informed consent was taken from all the patients.

Cell culture

Colorectal cell line of FHC (Cat# CRL-1831), HT29 (Cat# HCT-38), HCT8 (Cat#CCL-244), HCT116 (Cat# CCL-247), SW480 (Cat# CCL-228), SW620 (Cat# CCL-227), and RKO (Cat# CRL-2577) were purchased from Foleibao Biotechnology Development (Shanghai, China). For the use in experiments of the study, the cells were resuscitated and propagated less than 6 months. These cells were all cultured in RPMI 1640 medium (Cat# A1049101, Thermo Fisher Life Technologies Corporation; Grand Island, NY, USA) with 10% fetal bovine serum (Cat# 10091130, Invitrogen, MA, USA). The lentivirus with MYO1B oligonucleotides or MYO1B short hairpin RNA (shRNA) was purchased from GeneCopoeia (Guangzhou, China) and transfected as previously described (6). Exoenzyme C3 (E-C3) was

purchased from CytoSkeleton (USA, Cat# CT03-B).

RNA isolation, reverse transcription, and quantitative real-time PCR

Total RNA was extracted using Trizol (Invitrogen; Carlsbad, California). To quantify the transcription level of MYO1B, we subjected the total RNA to polyadenylation and reverse transcription (RT) using a ThermoScript^{TM} RT-PCR System (Invitrogen). Real-time polymerase chain reaction (PCR) analysis was performed according to the instruction of SYBR Green PCR master mix (Applied Biosystems; Foster City, California) on an ABI 7500HT system. We chose GAPDH snRNA as the endogenous control. All samples were normalized to internal controls, and fold changes were calculated by relative quantification ($2^{-\Delta\Delta CT}$). Real-time PCR for the target genes was performed as previously described (23). The primers used are shown in Table S1. When the MYO1B expression was higher than the average value, the patient was assigned to the MYO1B-high expression group. Otherwise, they were assigned to the MYO1B-low expression group.

Immunoblotting assay

For immunoblotting, the cultured cells were harvested, washed with phosphate-buffered saline (PBS), and lysed in a radioimmunoprecipitation assay (RIPA) buffer as described previously (6). The antibodies used were as follows: Rabbit antibodies against MYO1B (Cat# ab194356), ROCK2 (Cat# ab71598), phosphorylated-ROCK2 (Cat# ab182648), LIMK1 (Cat# ab81046), LIMK2 (Cat# ab97766), and RAC1 (Cat# ab155938) were purchased from Abcam (Shanghai, China). Rabbit antibodies against phosphorylated-LIMK1/2 (Cat# 3841), Cofilin (Cat# 5175), phosphorylated-Cofilin (Cat# 3311), phosphorylated-paxillin (Cat# 2542), CDC42 (Cat# 2462), FAK (Cat# 3285), and phosphorylated-FAK (Cat# 8556) were purchased from Cell Signaling Technology (USA). The mouse antibody against paxillin (Cat# 610619) was purchased from BD Transduction Laboratories (USA), the mouse antibody against RhoA (Cat# sc-166399) was purchased from Santa Cruz (USA), and the mouse antibody against Active-RhoA (Cat# 26904) was purchased from NewEast Biosciences (USA). The rabbit antibodies against GAPDH (Cat# 60004-1-Ig) were purchased from Proteintech (USA). All the antibodies were used at 1:1,000 dilutions. The membranes, probed with the indicated primary antibodies, were subjected to the appropriate horseradish peroxidase-conjugated secondary antibodies (anti-rabbit: Cat# 7074 and anti-mouse: Cat# 7076, Cell Signaling Technology, USA) and developed by enhanced chemiluminescence.

Immunohistochemical assay (IHC)

IHC was performed on the paraffin sections of the normal colorectal and CRC tissues as the labeled streptavidin-biotin (LSAB) protocol (Dako) using primary antibodies against MYO1B (Cat# ab194356, Abcam, Shanghai, China). The score of IHC staining were evaluated by two senior pathologists respectively. The percent positivity of MYO1B staining was scored from 0–4: 0 (0%), 1 (1–25%), 2 (26–50%), 3 (51–75%), and 4 (>75%). The staining intensity was scored on a 4-point scale: 0 (no staining observed in IHC), 1 (weak staining, light yellow staining can be observed), 2 (moderate staining, yellowish-brown staining was observed), and 3 (strong staining, brown staining was observed). Subsequently, the MYO1B expression score was calculated as the product of the percent positivity score and staining intensity score and ranged from 0–12. The final expression level of MYO1B was defined as low [0–5] or high [6–12].

Orthotopic xenograft CRC mouse model

SW480 (vehicle and MYO1B+) and HCT116 cells (Control and Sh-MYO1B) were suspended with PBS at a density of 1×10^6 cells/50 μL. Sixty 6-week-old Balb/c mice were randomly and equally divided into groups of veh, MYO1B+, Ctrl and Sh-MYO1B by simple randomization and they were anesthetized, and the cecum was exposed by laparotomy. In short, a small scratch (0.5–1 cm long) was incised on the skin, and we lifted abdominal wall musculature to open abdominal cavity for next step. Then we carefully isolated the cecum and a small gauze with warm saline-infused sterile was used to wet the cecum. The cells suspended in 50 μL PBS were carefully injected into the cecal wall. Check for leakage after remove the needle in the injection sit. Then the cecum was replaced in the abdominal cavity, and the abdominal wall and skin were sutured. *in vivo* imaging was performed on days 7, 14, and 28 after cell injection, and luciferin (150 mg/kg) (Cat# P1043, Caliper Life Science, Hopkinton, MA, USA) was intraperitoneally injected into each mouse 10 min before imaging. A Caliper IVIS Lumina II (Caliper Life Sciences, Hopkinton, MA, USA) was used for the bioluminescence imaging to monitor the tumor growth. Twenty-eight days

later, the mice were sacrificed, and the orthotopic xenograft CRC masses were measured and harvested for further hematoxylin-eosin staining (HE).

Animals experiments were performed under a project license granted by Ethics Committee of Zhujiang Hospital, Southern Medical University, in compliance with the Experimental Animal Center of Southern Medical University for the care and use of animals. A protocol was prepared before the study without registration.

Statistical analysis

SPSS v19.0 (SPSS, Chicago, IL, USA) was used for statistical analysis. The clinical data were analyzed using nonparametric tests (Wilcoxon and Mann-Whitney) and Kaplan-Meier and Cox Regression survival analyses. Difference between two groups was tested by Pearson's chi-squared (χ^2) test, unpaired Student's *t*-test, or paired *t*-test. All statistical tests were two-sided. Unless otherwise stated, data were expressed as mean ± SEMs.

Additional methods and material

Other methods can be found in the Supplementary file (Appendix 1).

Results

A higher MYO1B expression was associated with an increased risk of tumor metastasis and a poorer prognosis for CRC patients

We detected the transcriptional level of MYO1B in 50 pairs of fresh CRC and matched normal mucosa tissues and found that the MYO1B transcriptional level in 38 CRC tissues was significantly higher than in the paired adjacent normal tissues (*Figure 1A*). The Student's *t*-test confirmed that the MYO1B transcriptional level in the CRC tissues was statistically higher than in the normal mucosa tissues (*Figure 1B*), indicating that alteration of MYO1B transcription may be related to the incidence of CRC. Further Chi-square tests found that a high transcriptional level of MYO1B in CRC tissues was significantly associated with tumor metastasis and progression (*Figure 1C,1D*, Table S2). We also detected MYO1B protein expression in 101 CRC and 77 normal mucosa tissues and found that MYO1B expression in the CRC tissues was significantly higher than in the adjacent normal tissues (*Figure 1E*). The MYO1B staining score in CRC tissues was statistically higher than that in the normal mucosa tissues (*Figure 1F,1G*). The chi-square test for the IHC staining data also revealed that an increased expression of MYO1B was significantly associated with a high risk of lymph and distal metastasis (*Figure 1H,1I*, Table S3). Moreover, the Kaplan-Meier survival analysis showed that an increased expression of MYO1B was closely related to a poorer prognosis for CRC patients (*Figure 1J*). Further univariate and multivariate cox regression analyses confirmed MYO1B as an independent prognostic factor for CRC (Tables S4,S5). Taken together, our results indicated that MYO1B expression was increased in most CRC tissues, and this higher expression was positively associated with a greater risk of tumor incidence, metastasis, and a poorer prognosis for CRC patients.

MYO1B promoted the migration, invasion, and motility of CRC cells in vitro

We also investigated MYO1B expression in one normal epithelial cell line (FHC) and six CRC cell lines (SW480, RKO, SW620, HCT116, HCT8, and HT29). We found that MYO1B expression in five of the CRC cell lines (especially the HCT116 cell line) was significantly higher than in the normal epithelial cell line. However, the MYO1B expression in the SW480 cell line was statistically lower than that in the normal epithelial cell line (*Figure 2A*). Therefore, we chose the SW480 and HCT116 cell lines for further studies. Lentivirus with MYO1B oligonucleotides was used to overexpress MYO1B in the SW480 cell line (MYO1B+ group), while lentivirus with short hairpin RNA (shRNA) was used to silence the expression of MYO1B in the HCT116 cell line (sh-MYO1B group). An immunoblot assay was used to verify the construction of the MYO1B-overexpressed and silenced cell lines (*Figure 2B*). A transwell assay (with and without matrigel) showed that an increased MYO1B expression significantly promoted the migration and invasion ability of the SW480 cell line. The opposite result was achieved when MYO1B expression was silenced in the HCT116 cell line (*Figure 2C-2F*). A subsequent wound-healing assay also showed that overexpression of MYO1B dramatically promoted the motility of the SW480 cells, whereas a decreased MYO1B expression inhibited the motility of the HCT116 cells (*Figure 2G,2H*). Taken together, these results showed that MYO1B significantly promoted the migration, invasion, and motility of CRC

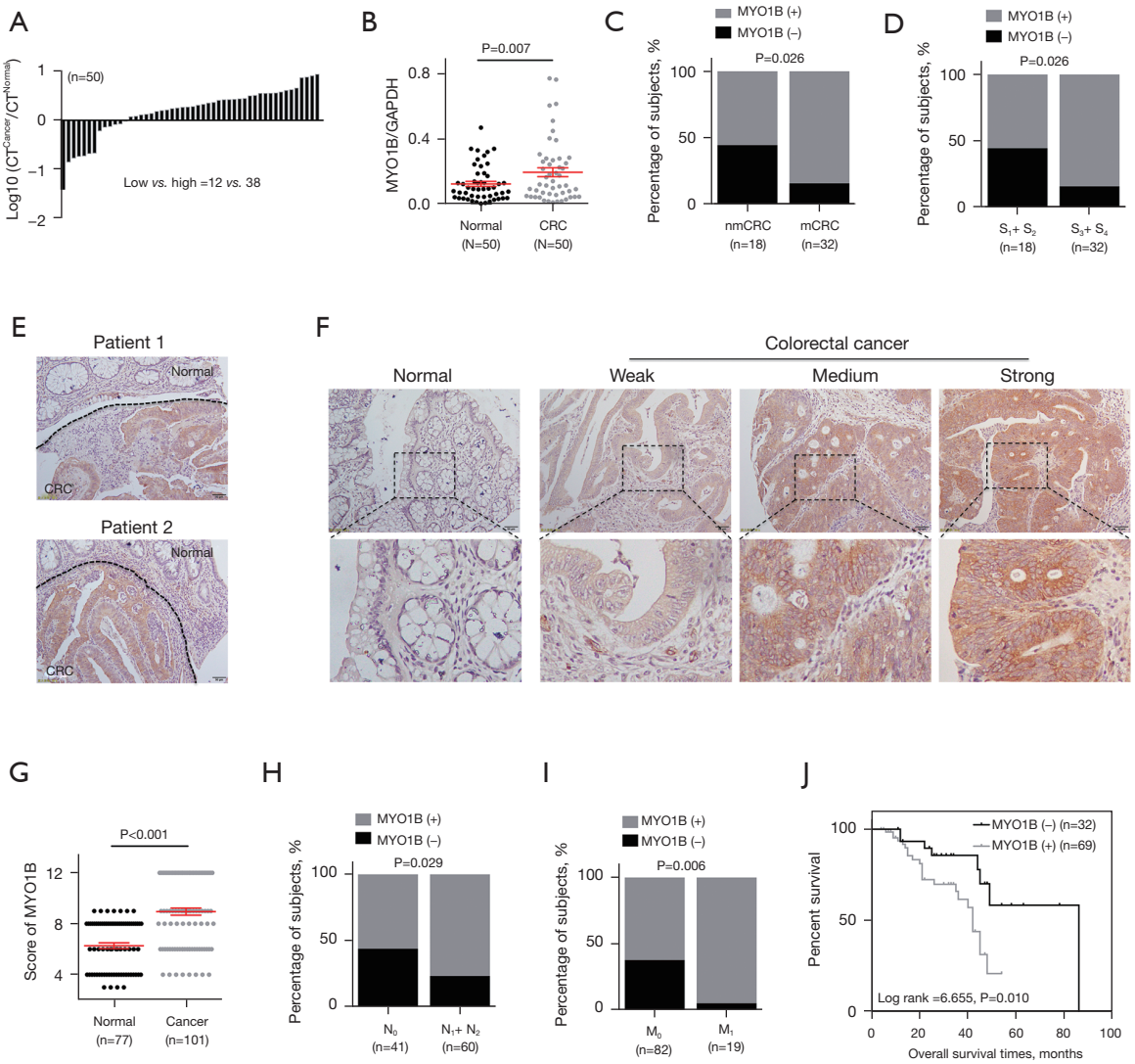

Figure 1 A high expression of MYO1B in colorectal cancer increases the risk of tumor metastasis and poor prognosis for patients. (A) Quantitative real-time PCR detection of the transcriptional level of MYO1B in fresh clinical tissues. Bars represent the ratio of MYO1B expression in CRC tissues (CTcancer, CRC tissues) to that in matched adjacent normal tissues (CTNormal, adjacent normal tissues). (B) The paired Student's *t*-test analysis of the difference between MYO1B transcription in fresh CRC and matched adjacent normal tissues. (C) Pearson's chi-squared (χ^2) test analysis of the relationship between MYO1B transcription and tumor metastasis, where "nmCRC" indicates non-metastatic CRC, and "mCRC" indicates metastatic CRC. (D) Pearson's chi-squared (χ^2) test analysis of the relationship between MYO1B transcription and tumor stage, where "S_1", "S_2", "S_3", and "S_4" indicate stage I, stage II, stage III, and stage IV, respectively. (E) Representative figures of the MYO1B protein expression in CRC and adjacent normal tissues by immunohistochemical staining. Shown at ×100 original magnification. (F) Representative figures of the different levels of MYO1B expression in CRC and normal mucosa tissues by immunohistochemical staining. Shown at ×100 original magnification. (G) Unpaired Student's *t*-test analysis of the difference between MYO1B expression in CRC and normal mucosa tissues in the paraffin CRC samples from Zhujiang Hospital. (H) The Pearson's chi-squared (χ^2) analysis of the relationship between MYO1B expression and tumor lymph classification in the paraffin CRC samples from Zhujiang Hospital. (I) The Pearson's chi-squared (χ^2) analysis of the relationship between MYO1B expression and tumor distal classification in the paraffin CRC samples from Zhujiang Hospital. (J) The Kaplan-Meier survival analysis of the paraffin CRC samples from Zhujiang Hospital. MYO1B (+), high MYO1B transcription. MYO1B (–), low MYO1B transcription. CRC, colorectal cancer.

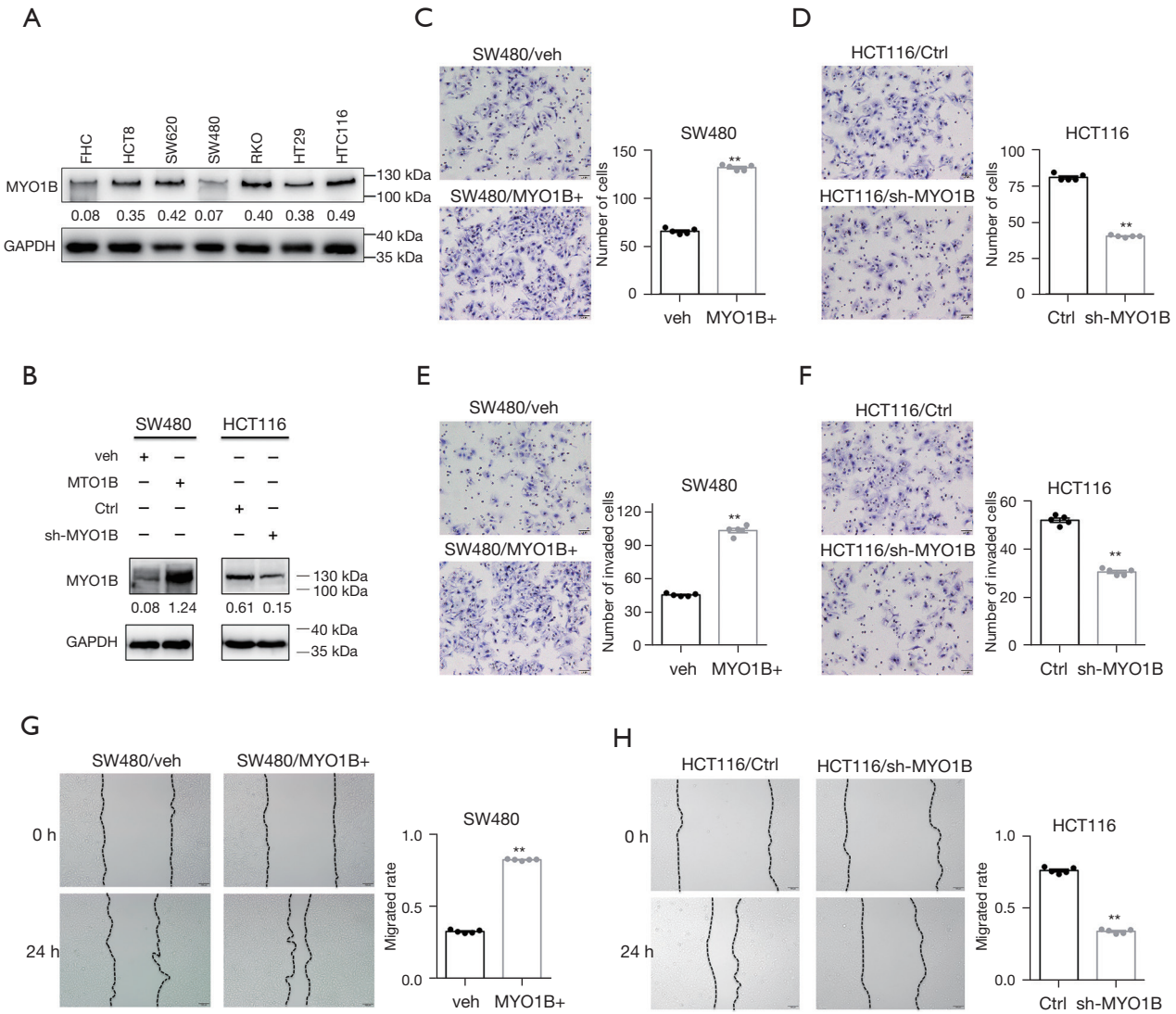

Figure 2 MYO1B promotes the migration, invasion, and motility of CRC cells *in vitro*. (A) Representative figures of the western blots for MYO1B expression in normal epithelial and colorectal cancer cell lines. The values under the membrane represent the expression of genes normalized to the expression of the reference gene GAPDH. (B) Representative figures of the western blots for MYO1B expression in cells transfected with lentivirus-MYO1B or lentivirus-shMYO1B. The values under the membrane represent the expression of genes normalized to the expression of the reference gene GAPDH. (C,D) Transwell assay without matrigel to investigate the migration property of CRC cells. Representative figures are in the left panel, and bars in the right panel are expressed as mean ± SEM. Cells were stained with crystal violet and counted. Scale bar: 200 μm. (E,F) Transwell assay with matrigel to investigate the invasion property of CRC cells. Representative figures are in the left panel, and bars in the right panel are expressed as mean ± SEM. Cells were stained with crystal violet and counted. Scale bar: 200 μm. (G,H) Wound-healing assay for investigating the motility of CRC cells. Representative figures are in the left panel, and bars in the right panel are expressed as mean ± SEM. **P<0.01 *vs.* control. CRC, colorectal cancer; Ctrl, control; Veh, vehicle.

cells *in vitro*.

MYO1B was associated with a higher risk of tumor metastasis and poor prognosis in CRC in vivo

An orthotopic xenograft CRC mouse model was used to investigate the effect of MYO1B on CRC metastasis and progression. Four weeks after cell injection, the *in vivo* bioluminescence imaging assay showed that 13 out of 15 mice had liver metastases in the SW480/MYO1B-overexpressed group compared with only 3 out of 15 mice in the SW480/control group (*Figure 3A*), with prolonged overall survival time (OS) in SW480/control group. Moreover, 11 out of 15 mice had liver metastases in the HCT116/control group compared with only 4 out of 15 mice in the HCT116/sh-MYO1B group (*Figure 3A*), with prolonged overall survival (OS) time in HCT116/sh-MYO1B group (*Figure 3B*). Notably, 2 weeks after cell injection, the *in vivo* bioluminescence imaging assay showed that six out of 15 mice had liver metastases in the SW480/MYO1B-overexpressed group compared with none of the mice in the SW480/control group. In the HCT116/control group, five out of 15 mice had liver metastases compared with only 1 out of 15 mice in the HCT116/sh-MYO1B group 2 weeks after cell injection. Representative figures of *in vivo* imaging in the orthotopic xenograft colorectal cancer mouse model in 1, 2 and 4 weeks (*Figure 3C*,*3D*). The HE staining assay revealed that the liver metastasis nodules in the SW480/MYO1B-overexpressed group were much larger than those in the SW480/control group (*Figure 3E*), whereas the liver metastasis nodules in the HCT116/sh-MYO1B group were much smaller than those in the HCT116/control group (*Figure 3F*). Overall, these results showed that an increased expression of MYO1B dramatically promoted liver metastasis in CRC and led to a poorer prognosis of mice *in vivo*.

MYO1B promoted F-actin rearrangement and activation of the ROCK2/LIMK/Cofilin axis in CRC cells

MYO1B is a well-known depolymerase for F-actin and plays an important role in cell migration by exerting and sustaining pN forces on F-actin (21). Therefore, we investigated the effect of MYO1B on F-actin depolymerization in CRC cells. Surprisingly, the immunofluorescence assay showed that an increased expression of MYO1B significantly promoted the rearrangement of F-actin in SW480 cells compared with the control group (*Figure 4A*), while a decreased expression of MYO1B had the opposite effect on F-actin rearrangement in the HCT116 cells (*Figure 4B*). An immunoblot assay revealed that overexpressing MYO1B promoted the phosphorylation of ROCK2, LIMK, and Cofilin in the SW480 cells, whereas silencing MYO1B inhibited their phosphorylation in the HCT116 cells, indicating that MYO1B promoted the activation of the ROCK2/LIMK/Cofilin axis (*Figure 4C*). Consistent changes in phosphorylated-LIMK and phosphorylated-Cofilin expressions were also found in a further immunofluorescence assay (*Figure 4D-4G*). Notably, the ROCK2/LIMK/Cofilin axis is a well-known F-actin rearrangement-related signaling pathway, and its activation indicated the promotion of F-actin rearrangement (24,25). Taken together, these results indicated that MYO1B might play an essential role in promoting F-actin rearrangement through the ROCK2/LIMK/Cofilin axis.

MYO1B promoted RhoA activation in CRC cells

Small GTPase members of the Rho superfamily are vital regulators of cell migration by mediating the activation of cytoskeleton rearrangement-related signaling, among which RhoA, CDC42 (Cell Division Cycle-42), and RAC1 are three known key members (25,26). We hypothesized that MYO1B might activate the ROCK2/LIMK/Cofilin axis through the Rho family small GTPase members, so we investigated the interaction of MYO1B with RhoA, CDC42, and RAC1 via an immunoprecipitation assay. In the HCT116 cell line, our results showed that MYO1B interacted with RhoA, but not CDC42 or RAC1 (*Figure 5A*,*5B*). An additional immunofluorescence assay showed strong co-localized signaling between MYO1B and RhoA in the HCT116 cells (*Figure 5C*). Further immunoblot assays showed that MYO1B had no effect on regulating the expression of RhoA (*Figure 5D*). However, the quantitative immunoprecipitation assay found that overexpressing MYO1B significantly increased the level of GTP-binding RhoA ($RhoA^{GTP}$) (*Figure 5E*), whereas silencing MYO1B decreased its level in HCT116 cells (*Figure 5F*). These results revealed that MYO1B played an essential role in promoting RhoA activation, which may explain the MYO1B-mediated promotion of the ROCK2/

A

Cell line	Treatment	Orthotopic tumor [n (%)]	Liver metastasis [n (%)]
SW480	veh	15 (100.0%)	3 (20.0%)
	MYO1B+	15 (100.0%)	13 (86.7%)
HCT116	Crl	15 (100.0%)	11 (73.3%)
	Sh-MYO1B	15 (100.0%)	4 (26.7%)

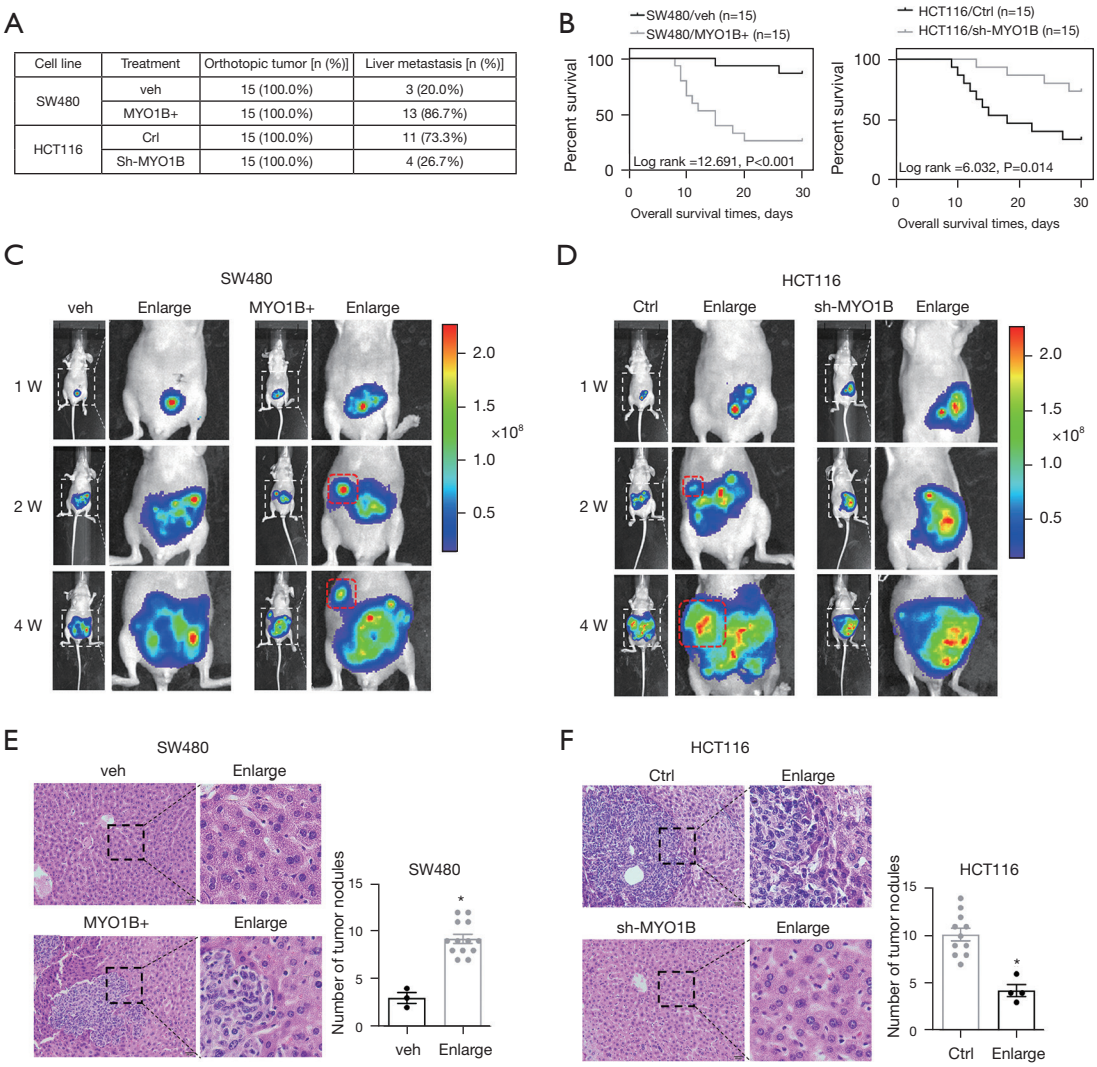

Figure 3 MYO1B promotes the risk of tumor metastasis and poor prognosis for CRC *in vivo*. (A) The rate of tumor formation and metastasis in the orthotopic xenograft mouse model. (B) The Kaplan-Meier survival analysis of the effect of MYO1B on CRC prognosis *in vivo*. (C,D) Representative figures of *in vivo* imaging in the orthotopic xenograft colorectal cancer mouse model. The square region of dotted lines indicates the CRC metastasis nodule in the liver; "w" indicates week. (E,F) HE staining of the CRC metastasis nodule in the liver. Representative figures are in the left panel, and bars in the right panel are expressed as mean ± SEM. Shown at ×400 original magnification. *P<0.05, **P<0.01, *vs.* control. CRC, colorectal cancer; Ctrl, control; Veh, vehicle.

LIMK/Cofilin axis and F-actin rearrangement.

MYO1B promoted the formation of migratory focal adhesions in CRC cells

It has been confirmed that the activation of RhoA also plays an important role in forming a migratory phenotype of focal adhesions, which are another vital factor in cell migration (27,28). Therefore, we further investigated the effect of MYO1B on focal adhesion assembly. Immunoblot assay showed that overexpressing MYO1B significantly promoted the phosphorylation level of FAK and paxillin in SW480 cells while silencing MYO1B inhibited their phosphorylation level (*Figure 5G*). Moreover, an immunofluorescence assay revealed that an increased expression of MYO1B dramatically promoted the formation of disassembled focal adhesions in SW480 cells. In contrast, a decreased MYO1B expression promoted the formation of

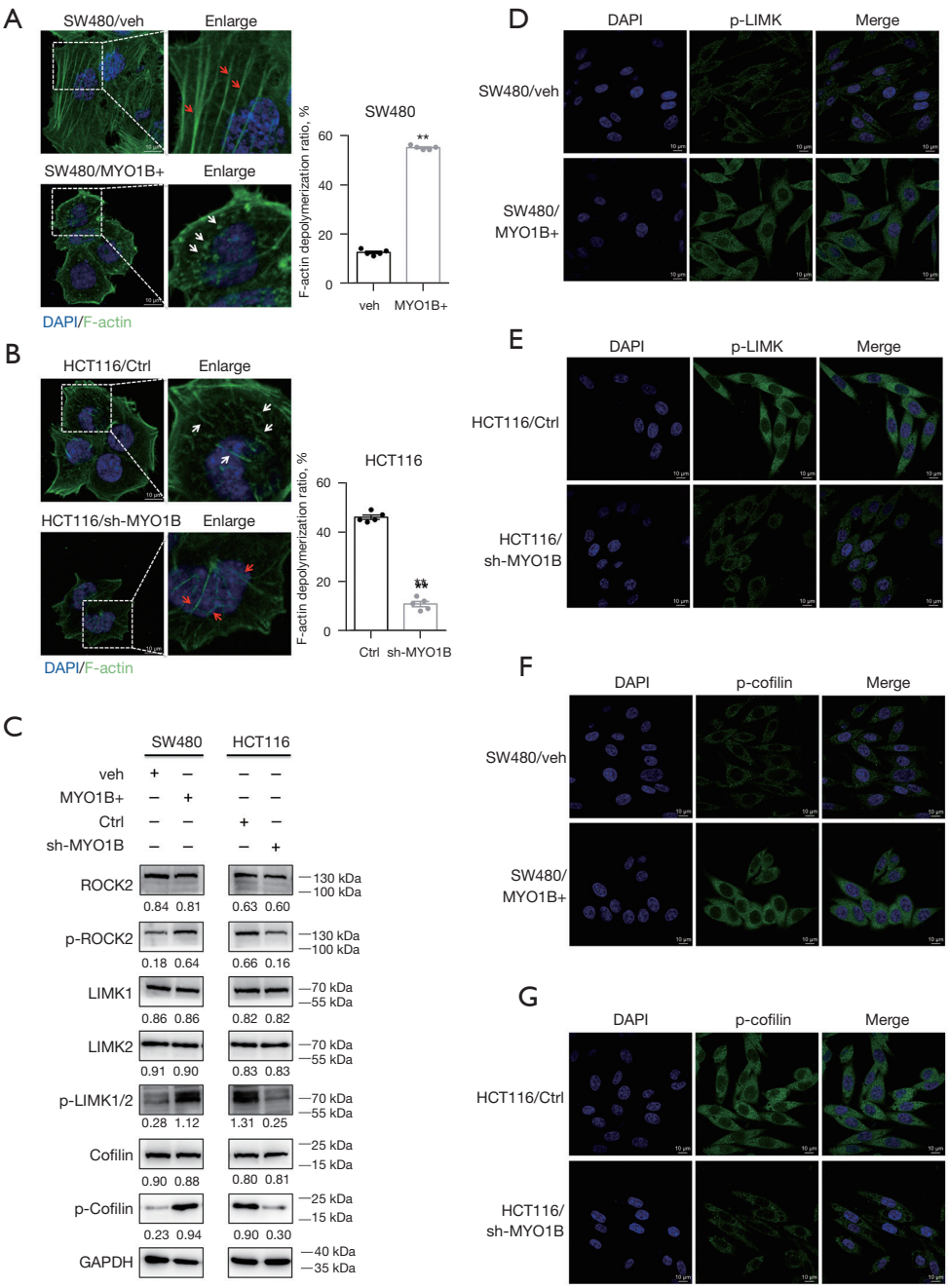

Figure 4 MYO1B promotes F-actin rearrangement and the activation of the ROCK2/LIMK/Cofilin axis in CRC cells. (A,B) Immunofluorescence assay of the rearrangement of F-actin. Representative figures are in the left panel, red arrows indicate the polymerization of F-actin, while white arrows indicate the depolymerization of F-actin. Bars in the right panel are expressed as mean ± SEM. (C) Representative figures of the western blots for the expression of the ROCK2/LIMK/Cofilin axis signatures in cells transfected with lentivirus-MYO1B or lentivirus-shMYO1B. The values under the membrane represent the expression of genes normalized to the expression of the reference gene GAPDH. (D,E) Representative figures of the immunofluorescence assay for the expression of p-LIMK. (F,G) Representative figures of the immunofluorescence assay for the expression of p-Cofilin. Shown at ×10,000 original magnification (A,B,D-G). **P<0.01 *vs.* control. CRC, colorectal cancer; Ctrl, control; Veh, vehicle.

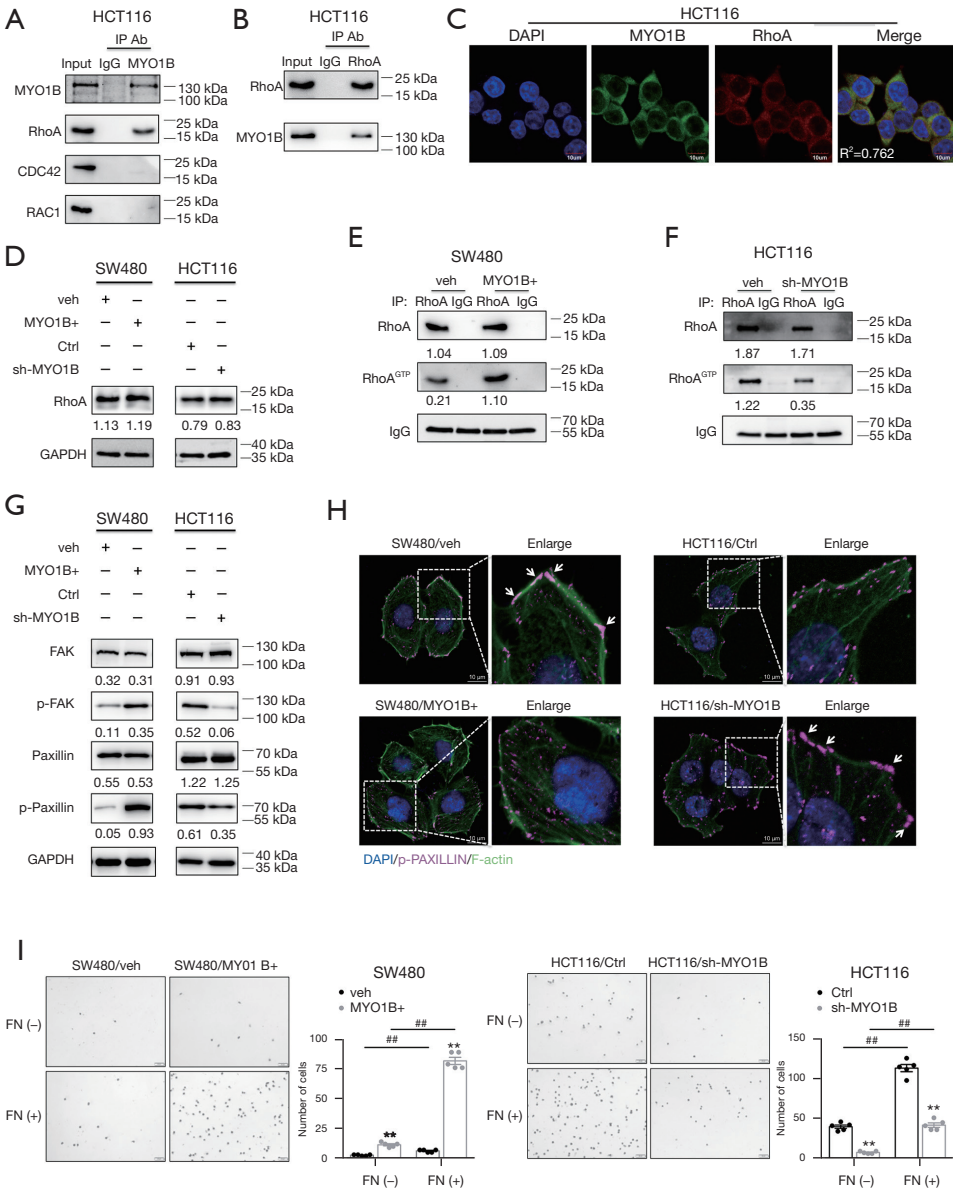

Figure 5 MYO1B promotes the activation of RhoA and the formation of migratory focal adhesions in CRC cells. (A) Representative figures of the co-immunoprecipitation assay on MYO1B to CDC42, RAC1, and RhoA. (B) Representative figures of the co-immunoprecipitation assay on RhoA to MYO1B. (C) Representative figures of the immunofluorescence assay on the co-localization of MYO1B and RhoA in CRC cells. (D) Representative figures of the western blots for RhoA expression in cells transfected with lentivirus-MYO1B or lentivirus-shMYO1B. The values under the membrane represent the expression of genes normalized to the expression of the reference gene GAPDH. (E,F) Representative figures of the co-immunoprecipitation assay for the expression of RhoA and GTP-binding RhoA ($RhoA^{GTP}$). (G) Representative figures of the western blots for the expression of the FAK/paxillin axis signatures in cells transfected with lentivirus-MYO1B or lentivirus-shMYO1B. The values under the membrane represent the expression of genes normalized to the expression of the reference gene GAPDH. Shown at ×10,000 original magnification. (H) Representative figures of the immunofluorescence assay on the formation of migratory focal adhesions. Shown at ×10,000 original magnification. (F) The fibronectin adhesive assay of the adhesive property of CRC cells. Representative figures are in the left panel, and bars in the right panel are expressed as mean ± SEM. (I) fibronectin adhesive assay showed the correlation between MYO1B expression and adhesive property in SW480 cells and HCT116 cells. Cells were fixed and stained with 1% crystal violet. Scale bar: 100 μm. **, P<0.01 *vs.* control; ##, P<0.01. CRC, colorectal cancer; Ctrl, control; Veh, vehicle.

assembled focal adhesions in HCT116 cells (*Figure 5H*). A fibronectin adhesive assay showed that an increased MYO1B expression significantly promoted the adhesive property of SW480 cells, while a decreased MYO1B expression had the opposite effect in HCT116 cells (*Figure 5I*). These findings strongly indicated that an increased expression of MYO1B significantly promoted the formation of migratory focal adhesions in CRC cells.

MYO1B promoted the migration, invasion, and motility of CRC cells by targeting RhoA

To further investigate the role of RhoA in MYO1B-mediated CRC cell migration, invasion, and motility, we inhibited the activation of RhoA by using exoenzyme-C3, a specific inhibitor of RhoA activation (29,30). A quantitative immunoprecipitation assay was used to verify the inhibition of exoenzyme-C3 on RhoA activation (*Figure 6A*). A transwell assay showed that inhibiting the activation of RhoA almost eliminated the effect of MYO1B on cell migration and invasion (*Figure 6B-6D*). A wound-healing assay also showed that inhibiting the activation of RhoA significantly reversed the effect of MYO1B on cell motility (*Figure 6E*, Figure S1). A fibronectin adhesive assay showed that exoenzyme-C3 dramatically eliminated the promotion of MYO1B on cell adhesive properties (*Figure 6F*). A further immunofluorescence assay showed that exoenzyme-C3 disturbed the MYO1B-mediated formation of migratory focal adhesions, as well as the F-actin rearrangement (*Figure 6G,6H*). Consistently, inhibiting RhoA activation substantially reversed the MYO1B-mediated alteration of the cytoskeleton polymerization (ROCK2, LIMK1/2, Cofilin) and the focal adhesion turnover (FAK, paxillin) signatures (*Figure 6I,6J*).

Discussion

CRC is the third most common malignancy worldwide, and 22% of patients present with metastatic disease and about 50% patients destine to develop metastasis which is associated with a dismal prognosis (31). Several targeted agents have emerged clinically such as Bevacizumab, Regorafenib and Fruquintinib (32-34). In addition to chemotherapy and immunotherapy, these agents have become the most common systemic therapies for metastatic patients (35). However, not all patients are sensitive to these agents (32-34). Because much is still unknown biochemically about CRC metastasis, it is of great clinical significance to explore other mechanism and new targets of CRC metastasis. In present study, we found MYO1B a potential target for CRC metastasis.

MYO1B is an important member of the Myosin-I class. It contains a motor domain at its N-terminus that binds F-actin in response to a light chain binding domain (LCBD) that, in turn, binds calmodulin (in most cases). MYO1B also has a Tail domain at the C-terminus that binds phosphoinositides (21,36). It is well established that MYO1B plays a vital role during cell migration, especially in cancer cells. Previous studies have found that MYO1B is commonly overexpressed in cervical (18), prostate (13), and head and neck cancer (19,20) and significantly increases the risk of tumor metastasis by promoting the migration, invasion, and motility properties of cancer cells. However, MYO1B's role in CRC metastasis, as well as its underlying mechanism, has remained unclear. This study demonstrated that MYO1B plays a crucial role in CRC metastasis by promoting the rearrangement of F-actin and the formation of migratory focal adhesions. Our findings strongly suggest that MYO1B may be a valid biomarker for predicting the risk of tumor metastasis and poor prognosis in CRC patients.

To clarify the exact role of MYO1B during cell migration, we carried out many *in vitro* and *in vivo* biological experiments. Our results showed that MYO1B significantly promoted the migration, invasion, and motility of CRC cells *in vitro*. Interestingly, we found that downregulating MYO1B dramatically decreased the incidence of liver metastasis in CRC *in vivo*, as well as the number of liver metastasis nodules. These findings are consistent with previous studies of cervical (18) and head and neck cancer (19,20). Our results indicate that MYO1B may also be a potential therapeutic target for patients with a high risk of tumor metastasis. Further investigation of the underlying mechanism involved in the aberrant overexpression of MYO1B in CRC cells is necessary.

Previous studies have confirmed that MYO1B is an F-actin depolymerase and plays a significant role in promoting cell migration by exerting and sustaining forces on F-actin during its depolymerization (21,37). In the present study, we surprisingly found that MYO1B significantly promoted the F-actin rearrangement of CRC cells, which involves the polymerization and depolymerization of F-actin, signifying that MYO1B may have a direct or indirect role in promoting F-actin polymerization. Indeed, further investigation found that MYO1B significantly promoted activation of the ROCK2/LIMK/Cofilin axis, which is a crucial trigger for F-actin polymerization (25,38,39). Accordingly,

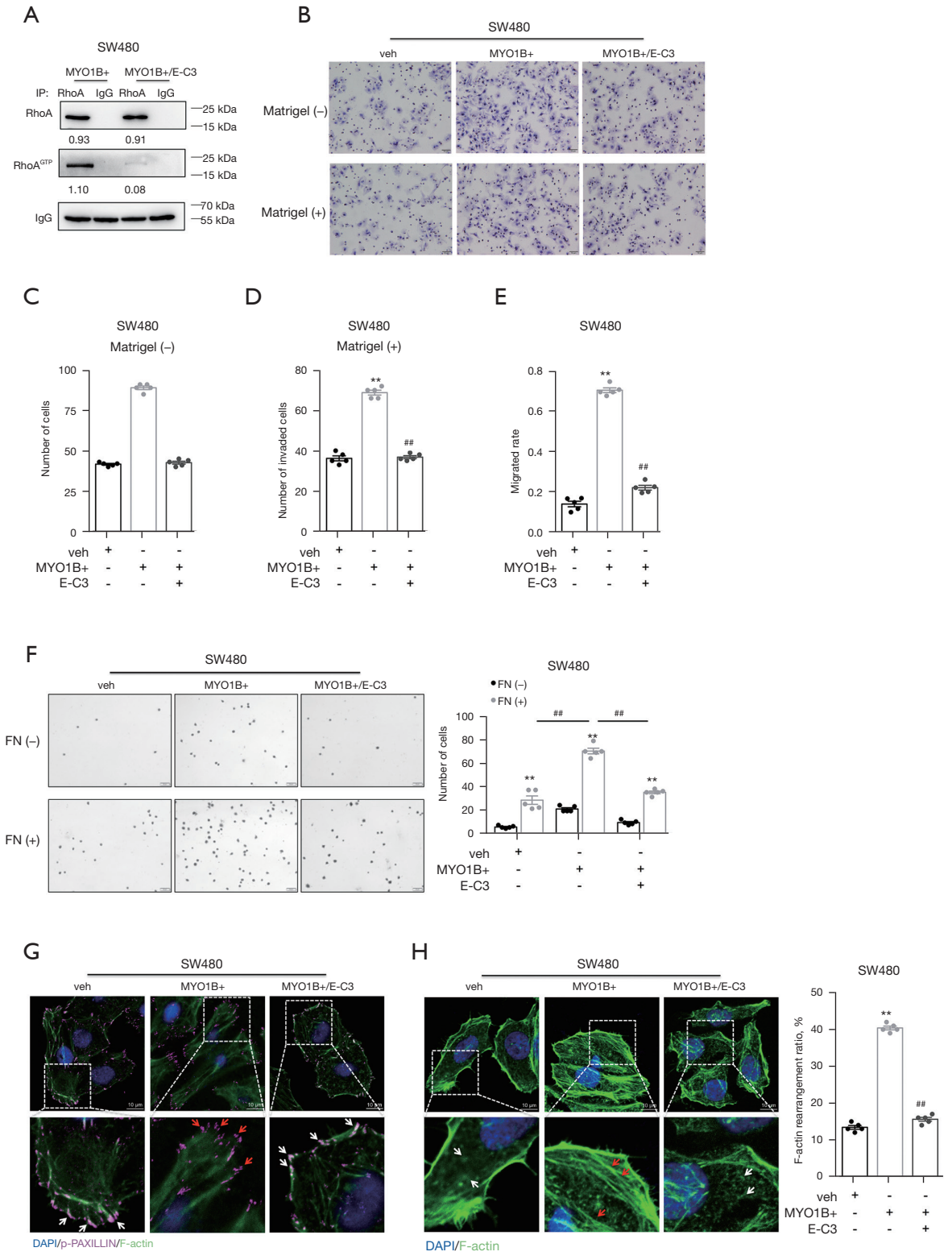

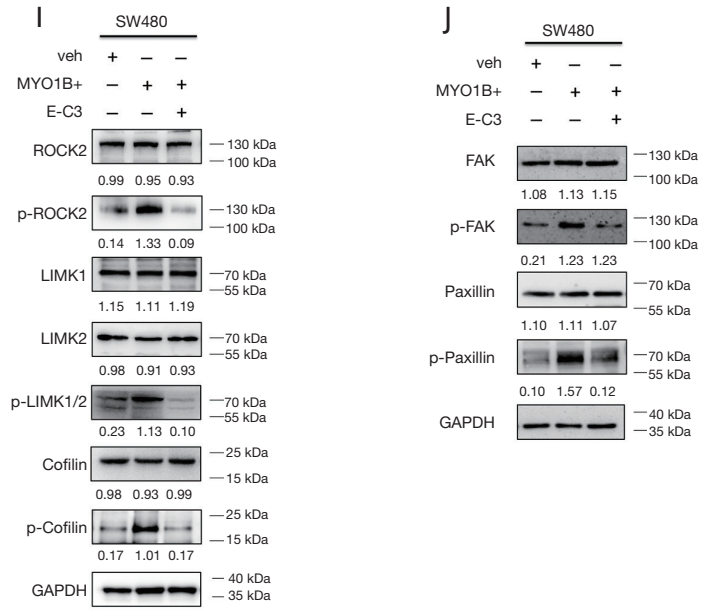

Figure 6 MYO1B promotes the migration, invasion, and motility of CRC cells by targeting RhoA. (A) Representative figures of the immunoprecipitation assay for the expression of RhoA and GTP-binding RhoA ($RhoA^{GTP}$) in cells treated with exoenzyme-C3, where "E-C3" indicates exoenzyme-C3. (B) Representative figures of the transwell assay with and without matrigel. Cells were stained with crystal violet and counted. Scale bar: 200μm. (C) Bars are expressed as mean ± SEM, indicating the number of migrating cells in the transwell assay without matrigel. (D) Bars are expressed as mean ± SEM, indicating the number of invading cells in the transwell assay with matrigel. (E) Bars are expressed as mean ± SEM, indicating the migration rate of cells in the wound-healing assay. (F) The fibronectin adhesive assay of the adhesive property of CRC cells. Cells were fixed and stained with 1% crystal violet. Scale bar: 100 μm. Representative figures are in the left panel, and bars in the right panel are expressed as mean ± SEM. (G) Representative figures of the immunofluorescence assay on the formation of migratory focal adhesions. Shown at ×10,000 original magnification. (H) The immunofluorescence assay of the rearrangement of F-actin. Representative figures are in the left panel, red arrows indicate the polymerization of F-actin, while white arrows indicate the depolymerization of F-actin. Bars in the right panel are expressed as mean ± SEM. Shown at ×10,000 original magnification. (I) Representative figures of the western blots for the expression of the ROCK2/LIMK/Cofilin axis signatures. The values under the membrane represent the expression of genes normalized to the expression of the reference gene GAPDH. (J) Representative figures of the western blots for the expression of the FAK/paxillin axis signatures. The values under the membrane represent the expression of genes normalized to the expression of the reference gene GAPDH. **, P<0.01 *vs.* control. ##, P<0.01. Ctrl, control; Veh, vehicle.

we suggest that MYO1B may play a key role in F-actin polymerization, even though time-lapse detection of F-actin polymerization was not provided in our study. In addition, it is conceivable that factors that concurrently promote F-actin polymerization and depolymerization are much more favorable for cell migration because they can effectively accelerate the cycle of F-actin rearrangement. Thus, we consider that a high expression of MYO1B in CRC tumor cells presents a crucial risk factor for metastasis.

It is widely recognized that small GTPase members of the Rho superfamily are the key regulators for F-actin polymerization, especially CDC42, RAC1, and RhoA (25,40,41). In the present study, we found that MYO1B significantly promoted the activation of RhoA, but not CDC42 or RAC1. Notably, we also found that MYO1B promoted the activation of ROCK2, which has been defined as a key downstream effector of RhoA in many studies (26,29,38). Further recovery experiments showed that inhibiting the activation of RhoA mostly eliminated the effect of MYO1B on cell migration, invasion, and motility properties, as well as F-actin depolymerization. Thus, we consider that MYO1B may promote the migration, invasion, and motility of CRC cells through F-actin rearrangement by targeting RhoA activation.

It has also been well demonstrated that the activation of RhoA plays a vital role in promoting the formation of migratory focal adhesions, another well-known factor for cell migration (27,42). Thus, we further investigated the role of MYO1B in focal adhesion formation in CRC cells. Our results showed that MYO1B significantly promoted the formation of migratory focal adhesions and enhanced the adhesive property of CRC cells. Moreover, our recovery experiments showed that inhibiting the activation of RhoA significantly eliminated the effect of MYO1B on the formation of migratory focal adhesions and the promotion of the adhesive property of CRC cells. Thus, MYO1B also appears to play a vital role in promoting the formation of migratory focal adhesions, which may be another important mechanism underlying MYO1B-mediated cell migration.

Focal adhesions are F-actin binding attachments in cells and provide the dynamic fulcrum for the F-actin architecture (43). There is a preferential ability for their formation at the leading edge of the cell membrane along with cell movement (44). Although some evidence points to the existence of a cytoskeletal complex that regulates the formation of adhesive complexes, its specific molecules have not been well identified. A previous study has pointed to the existence of a cytoskeletal complex that precedes the incorporation of focal adhesions (45). Interestingly, MYO1B may bind to and depolymerize F-actin to form a disassembled F-actin/MYO1B complex in cells. Moreover, our study found that MYO1B also played a crucial role in promoting the formation of migratory focal adhesions. Thus, we consider that MYO1B may be the key component of the cytoskeletal complex accounting for the incorporation of initial focal adhesions by targeting RhoA.

Conclusions

The present study found that MYO1B plays a key role in CRC tumor metastasis by targeting the activation of RhoA. MYO1B may not only be a valid biomarker for predicting the risk of metastasis and poor prognosis in CRC but may also be a potential therapeutic target for patients with a high risk of tumor metastasis.

Acknowledgments

Funding: This work was supported by the Natural Science Foundation of China (No. 8197032867) and the Science and Technology Planning Project of Guangdong Province (No. 2019B030316011).

Footnote

Reporting Checklist: The authors have completed the ARRIVE reporting checklist. Available at https://dx.doi.org/10.21037/atm-21-4702

Data Sharing Statement: Available at https://dx.doi.org/10.21037/atm-21-4702

Conflicts of Interest: All authors have completed the ICMJE uniform disclosure form (available at https://dx.doi.org/10.21037/atm-21-4702). The authors declare that this work was supported by the Natural Science Foundation of China (No. 8197032867) and the Science and Technology Planning Project of Guangdong Province (No. 2019B030316011). The authors have no other conflicts of interest to declare.

Ethical Statement: The authors are accountable for all aspects of the work in ensuring that questions related to the accuracy or integrity of any part of the work are appropriately investigated and resolved. All procedures performed in this study involving human participants were in accordance with the Declaration of Helsinki (as revised in 2013). The study was approved by Ethics Committee of Zhujiang Hospital of Southern Medical University and informed consent was taken from all the patients. Animals experiments were performed under a project license granted by Ethics Committee of Zhujiang Hospital, Southern Medical University, in compliance with the Experimental Animal Center of Southern Medical University for the care and use of animals. A protocol was prepared before the study without registration.

References

1. Ferlay J, Shin HR, Bray F, et al. Estimates of worldwide burden of cancer in 2008: GLOBOCAN 2008. Int J

Cancer 2010;127:2893-917.
2. Hu JL, Wang W, Lan XL, et al. CAFs secreted exosomes promote metastasis and chemotherapy resistance by enhancing cell stemness and epithelial-mesenchymal transition in colorectal cancer. Mol Cancer 2019;18:91.
3. Jackstadt R, van Hooff SR, Leach JD, et al. Epithelial NOTCH Signaling Rewires the Tumor Microenvironment of Colorectal Cancer to Drive Poor-Prognosis Subtypes and Metastasis. Cancer Cell 2019;36:319-336.e7.
4. Yang X, Zhang S, He C, et al. METTL14 suppresses proliferation and metastasis of colorectal cancer by down-regulating oncogenic long non-coding RNA XIST. Mol Cancer 2020;19:46.
5. Zheng K, Yu J, Chen Z, et al. Ethanol promotes alcohol-related colorectal cancer metastasis via the TGF-β/RUNX3/Snail axis by inducing TGF-β1 upregulation and RUNX3 cytoplasmic mislocalization. EBioMedicine 2019;50:224-37.
6. Zheng K, Zhou X, Yu J, et al. Epigenetic silencing of miR-490-3p promotes development of an aggressive colorectal cancer phenotype through activation of the Wnt/β-catenin signaling pathway. Cancer Lett 2016;376:178-87.
7. Fu T, Coulter S, Yoshihara E, et al. FXR Regulates Intestinal Cancer Stem Cell Proliferation. Cell 2019;176:1098-1112.e18.
8. Liao W, Overman MJ, Boutin AT, et al. KRAS-IRF2 Axis Drives Immune Suppression and Immune Therapy Resistance in Colorectal Cancer. Cancer Cell 2019;35:559-572.e7.
9. Tilg H, Adolph TE, Gerner RR, et al. The Intestinal Microbiota in Colorectal Cancer. Cancer Cell 2018;33:954-64.
10. Shao Z, Cai Y, Xu L, et al. Loss of the 14-3-3σ is essential for LASP1-mediated colorectal cancer progression via activating PI3K/AKT signaling pathway. Sci Rep 2016;6:25631.
11. Pretzsch E, Bösch F, Neumann J, et al. Mechanisms of Metastasis in Colorectal Cancer and Metastatic Organotropism: Hematogenous versus Peritoneal Spread. J Oncol 2019;2019:7407190.
12. Biber G, Ben-Shmuel A, Sabag B, et al. Actin regulators in cancer progression and metastases: From structure and function to cytoskeletal dynamics. Int Rev Cell Mol Biol 2020;356:131-96.
13. Makowska KA, Hughes RE, White KJ, et al. Specific Myosins Control Actin Organization, Cell Morphology, and Migration in Prostate Cancer Cells. Cell Rep 2015;13:2118-25.
14. Brzeska H, Koech H, Pridham KJ, et al. Selective localization of myosin-I proteins in macropinosomes and actin waves. Cytoskeleton (Hoboken) 2016;73:68-82.
15. Bond LM, Brandstaetter H, Kendrick-Jones J, et al. Functional roles for myosin 1c in cellular signaling pathways. Cell Signal 2013;25:229-35.
16. Kim SV, Flavell RA. Myosin I: from yeast to human. Cell Mol Life Sci 2008;65:2128-37.
17. McConnell RE, Tyska MJ. Leveraging the membrane - cytoskeleton interface with myosin-1. Trends Cell Biol 2010;20:418-26.
18. Zhang HR, Lai SY, Huang LJ, et al. Myosin 1b promotes cell proliferation, migration, and invasion in cervical cancer. Gynecol Oncol 2018;149:188-97.
19. Chapman BV, Wald AI, Akhtar P, et al. MicroRNA-363 targets myosin 1B to reduce cellular migration in head and neck cancer. BMC Cancer 2015;15:861.
20. Ohmura G, Tsujikawa T, Yaguchi T, et al. Aberrant Myosin 1b Expression Promotes Cell Migration and Lymph Node Metastasis of HNSCC. Mol Cancer Res 2015;13:721-31.
21. Pernier J, Kusters R, Bousquet H, et al. Myosin 1b is an actin depolymerase. Nat Commun 2019;10:5200.
22. Köster DV, Mayor S. Cortical actin and the plasma membrane: inextricably intertwined. Curr Opin Cell Biol 2016;38:81-9.
23. Wang H, An H, Wang B, et al. miR-133a represses tumour growth and metastasis in colorectal cancer by targeting LIM and SH3 protein 1 and inhibiting the MAPK pathway. Eur J Cancer 2013;49:3924-35.
24. Gong H, Zhou L, Khelfat L, et al. Rho-Associated Protein Kinase (ROCK) Promotes Proliferation and Migration of PC-3 and DU145 Prostate Cancer Cells by Targeting LIM Kinase 1 (LIMK1) and Matrix Metalloproteinase-2 (MMP-2). Med Sci Monit 2019;25:3090-9.
25. Zhu GF, Xu YW, Li J, et al. Mir20a/106a-WTX axis regulates RhoGDIa/CDC42 signaling and colon cancer progression. Nat Commun 2019;10:112.
26. He M, Cheng Y, Li W, et al. Vascular endothelial growth factor C promotes cervical cancer metastasis via up-regulation and activation of RhoA/ROCK-2/moesin cascade. BMC Cancer 2010;10:170.
27. Zhang H, Schaefer A, Wang Y, et al. Gain-of-Function RHOA Mutations Promote Focal Adhesion Kinase Activation and Dependency in Diffuse Gastric Cancer. Cancer Discov 2020;10:288-305.
28. Zeng Y, Cao Y, Liu L, et al. SEPT9_i1 regulates human breast cancer cell motility through cytoskeletal and RhoA/FAK signaling pathway regulation. Cell Death Dis

2019;10:720.
29. Schollenberger L, Gronemeyer T, Huber CM, et al. RhoA regulates peroxisome association to microtubules and the actin cytoskeleton. PLoS One 2010;5:e13886.
30. Li G, Liu L, Shan C, et al. RhoA/ROCK/PTEN signaling is involved in AT-101-mediated apoptosis in human leukemia cells in vitro and in vivo. Cell Death Dis 2014;5:e998.
31. Tsilimigras DI, Brodt P, Clavien PA, et al. Liver metastases. Nat Rev Dis Primers 2021;7:27.
32. Emmanouilides C, Sfakiotaki G, Androulakis N, et al. Front-line bevacizumab in combination with oxaliplatin, leucovorin and 5-fluorouracil (FOLFOX) in patients with metastatic colorectal cancer: a multicenter phase II study. BMC Cancer 2007;7:91.
33. Strumberg D, Scheulen ME, Schultheis B, et al. Regorafenib (BAY 73-4506) in advanced colorectal cancer: a phase I study. Br J Cancer 2012;106:1722-7.
34. Li J, Qin S, Xu RH, et al. Effect of Fruquintinib vs Placebo on Overall Survival in Patients With Previously Treated Metastatic Colorectal Cancer: The FRESCO Randomized Clinical Trial. JAMA 2018;319:2486-96.
35. Provenzale D, Ness RM, Llor X, et al. NCCN Guidelines Insights: Colorectal Cancer Screening, Version 2.2020. J Natl Compr Canc Netw 2020;18:1312-20.
36. McIntosh BB, Ostap EM. Myosin-I molecular motors at a glance. J Cell Sci 2016;129:2689-95.
37. Pyrpassopoulos S, Arpağ G, Feeser EA, et al. Force Generation by Membrane-Associated Myosin-I. Sci Rep 2016;6:25524.
38. Fiedler SE, Bajpai M, Carr DW. Identification and characterization of RHOA-interacting proteins in bovine spermatozoa. Biol Reprod 2008;78:184-92.
39. Iobbi C, Korte M, Zagrebelsky M. Nogo-66 Restricts Synaptic Strengthening via Lingo1 and the ROCK2-Cofilin Pathway to Control Actin Dynamics. Cereb Cortex 2017;27:2779-92.
40. Kim JG, Islam R, Cho JY, et al. Regulation of RhoA GTPase and various transcription factors in the RhoA pathway. J Cell Physiol 2018;233:6381-92.
41. Ge J, Burnier L, Adamopoulou M, et al. RhoA, Rac1, and Cdc42 differentially regulate αSMA and collagen I expression in mesenchymal stem cells. J Biol Chem 2018;293:9358-69.
42. Nardone G, Oliver-De La Cruz J, Vrbsky J, et al. YAP regulates cell mechanics by controlling focal adhesion assembly. Nat Commun 2017;8:15321.
43. Lauffenburger DA, Horwitz AF. Cell migration: a physically integrated molecular process. Cell 1996;84:359-69.
44. Izzard CS, Lochner LR. Formation of cell-to-substrate contacts during fibroblast motility: an interference-reflexion study. J Cell Sci 1980;42:81-116.
45. Izzard CS. A precursor of the focal contact in cultured fibroblasts. Cell Motil Cytoskeleton 1988;10:137-42.

(English Language Editor: D. Fitzgerald)

Cite this article as: Xie L, Huang H, Zheng Z, Yang Q, Wang S, Chen Y, Yu J, Cui C. MYO1B enhances colorectal cancer metastasis by promoting the F-actin rearrangement and focal adhesion assembly via RhoA/ROCK/FAK signaling. Ann Transl Med 2021;9(20):1543. doi: 10.21037/atm-21-4702

Materials and methods

Cell migration and invasion analysis

The cells were maintained in a serum-containing growth medium for 48–72 h and then maintained in a serum-free medium for 24 h. The cells (1×105 cells/100 µL) were added to 8-µm pore transwell and matrigel chamber plates (Corning Star, Cambridge, Massachusetts). The bottom chamber was prepared using 10% fetal bovine serum as the chemoattractant. Cells were maintained at 37 ℃ and allowed to migrate through the porous membrane or the matrigel for 48 and 72 h, respectively. Fixation/staining solution (0.1% crystal violet, 1% formalin, and 20% ethanol) were used to fix and stain those cells that stuck to the lower surface of the membrane. The cells were counted under a microscope in five randomly selected fields with scale bar of 200 µm. At least five chambers from experiments in triplicate were analyzed.

Cell adhesion assay

Twenty-four-well plates coated with Fibronectin (FN, BD Biosciences, USA) were incubated for 1 h at 37 ℃. After blocking with 1% BSA, 3×10^4 cells were seeded in each well and incubated at 37 ℃ for 30 min. Then cells were fixed with 4% paraformaldehyde and stained with 0.1% crystal violet, and randomly select 5 visual fields in microscope and count the cells.

Cell motility assay

Confluent monolayers of cells were cultured in a serum-containing medium for 48–72 h and followed by 24-hour culture in serum-free medium. The monolayers were scratched by 1,000-µL plastic pipette tip followed by 48-hour culture in a serum-free medium and wounded cells photographed under an inverted phase-contrast microscope. Three different points were marked on the plate, and the distance between each point and the edge of the scratch wound was measured before and after cell migration. The mean migration distance (µm) was calculated by subtracting the length after 48 h from that at 0 h. The result was expressed as a migration index, i.e., the distance migrated by the treated cells compared with the distance migrated by the control cells. Experiments were carried out in triplicate and repeated at least five times.

Immunofluorescence assay

Cells were cultured on coverslips for 12 h, and then 4% paraformaldehyde was used to fix cells for 30 min, followed by 15-min treatment of 0.5% Triton X-100. The reaction was blocked with 10% normal blocking serum at room temperature for 15 min, the slides were incubated with rabbit antibodies to phosphorylated-LIMK2 and phosphorylated-cofilin (1:150) (Cell Signaling Technology; Danvers, Massachusetts) and rabbit antibodies to paxillin (1:100) (BD Transduction Laboratories, USA) at 4 ℃ overnight. This was followed by thrice PBS rinsing. The coverslips were then incubated with a fluorescein isothiocyanate (FITC)-conjugated anti-rabbit or mouse stain and Texas Red-conjugated anti-mouse or –rabbit antibodies (1:200) (SantaCruz Biotech) for 30 min at room temperature, then stained with 6-diamidino-2-phenylindole (DAPI, Invitrogen).

Co-immunoprecipitation assay

Cells were harvested and washed three times with chilled PBS, then lysed in IP Lysis Buffer (Pierce, USA) with a protease and phosphatase inhibitor cocktail (Sigma, USA). The protein was quantified by using a BCA Protein Assay Kit (KeyGen, Biotechnology, China), then diluted into 1 mg/mL with chilled wash buffer (with protease and phosphatase inhibitor), and divided into two equal parts, to which were added mouse anti-MYO1B or mouse anti-RhoA antibody (3–4 µg) (Santa Cruz, USA) and the same amount of rabbit IgG (Beyotime, China), respectively, rotated slowly and incubated overnight at 4 ℃. Protein A agarose beads were washed twice with cold wash buffer and added to the two parts of protein based on 20 µL for every 1 mL of total protein, then incubated for 4–6 h at 4 ℃ with low-speed rotation. Afterward, the protein mixture was washed three times with 500 µL chilled wash buffer (containing protease and phosphatase inhibitor). The protein mixtures were diluted with wash buffer. After heat denaturation in 10% SDS-PAGE sample loading buffer, the protein samples were subjected to western blot assay.

https://dx.doi.org/10.21037/atm-21-4702

Animals

Mice were 6-week-old and purchased from Experimental Animal Center of Southern Medical University (GuangZhou, China). The body weight, feeding behavior, and motor activity of animals were monitored as indicators of general health. Mice were kept under specific pathogen-free conditions in the Experimental Animal Center of Southern Medical University. Experiments were performed under a project license granted by Ethics Committee of Zhujiang Hospital, Southern Medical University, in compliance with the Experimental Animal Center of Southern Medical University for the care and use of animals.

Table S1 RT-PCR primer sequences for human genes

Gene	Forward primer	Reverse primer	Product length
MYO1B	GCTGGAGACCATGGCCAAAA	TCCTCCTAGTGGATCGCCTT	559 bp
GAPDH	GGAGCGAGATCCCTCCAAAAT	GGCTGTTGTCATACTTCTCATGG	197 bp

Table S2 Correlation of demographic characteristics and MYO1B transcription among 50 CRC patients

Characteristics	Total (n)	MYO1B		P value[1]
		Low [n (%)]	High [n (%)]	
Sex				0.007
Female	19	9 (47.4)	10 (52.6)	
Male	31	4 (12.9)	27 (87.1)	
Age at diagnosis (year)				0.050
≤50	9	0 (0.0)	9 (100.0)	
>50	41	13 (31.7)	28 (68.3)	
Tumor location				0.509
Right colon	27	6 (22.2)	21 (77.8)	
Left colon	23	7 (30.4)	16 (69.6)	
T classification				0.007
Tis + T0	0	0 (0.0)	0 (0.0)	
T1 + T2	19	9 (47.4)	10 (52.6)	
T3 + T4	31	4 (12.9)	27 (87.1)	
N classification				0.004
N0	18	9 (50.0)	9 (50.0)	
N1 + N2	32	4 (12.5)	17 (87.5)	
M classification				0.148
M0	39	12 (30.8)	27 (69.2)	
M1	11	1 (9.1)	10 (90.9)	
Stage				0.026
S1 + S2	18	8 (44.4)	10 (55.6)	
S3 + S4	32	5 (15.6)	27 (84.4)	

[1], Pearson χ^2 test of independence between covariables and MYO1B transcription.

https://dx.doi.org/10.21037/atm-21-4702

Table S3 Correlation of demographic characteristics and MYO1B expression among 101 CRC patients

Characteristics	Total (n)	MYO1B		P value[1]
		Low [n (%)]	High [n (%)]	
Sex				0.386
Female	41	11 (26.8)	30 (73.2)	
Male	60	21 (35.0)	39 (65.0)	
Age at diagnosis (year)				0.453
≤50	27	7 (25.9)	20 (74.1)	
>50	74	25 (33.8)	49 (66.2)	
Stage				0.053
S1 + S2	31	14 (45.2)	17 (54.8)	
S3 + S4	70	18 (25.7)	52 (74.3)	
T classification				0.739
Tis + T0	0	0 (0.0)	0 (0.0)	
T1 + T2	11	3 (27.3)	8 (72.7)	
T3 + T4	90	29 (32.2)	61 (67.8)	
N classification				0.029
N0	41	18 (43.9)	23 (56.1)	
N1 + N2	60	14 (23.3)	46 (76.7)	
M classification				0.006
M0	82	31 (37.8)	51 (62.2)	
M1	19	1 (5.3)	18 (94.3)	

[1], Pearson χ^2 test of independence between covariables and MYO1B expression

Table S4 Univariate cox regression analysis of factors associated with overall survival in colorectal cancer patients

	Exp(B)	95% CI for Exp(B)		P value
		Lower	Upper	
Sex	1.464	0.689	3.109	0.322
Age	1.009	0.979	1.040	0.556
T	2.072	0.493	8.704	0.320
N	1.663	0.799	3.457	0.174
M	1.862	0.793	4.373	0.153
Chemotherapy	0.775	0.382	1.575	0.482
MYO1B	1.205	1.054	1.377	0.006

https://dx.doi.org/10.21037/atm-21-4702

Table S5 Multivariate cox regression analysis of factors associated with overall survival in colorectal cancer patients

	Exp(B)	95% CI for Exp(B)		P value
		Lower	Upper	
Sex	1.449	0.651	3.228	0.364
Age	1.014	0.983	1.046	0.385
T	1.250	0.659	2.368	0.495
N	1.372	0.619	3.041	0.436
M	0.983	0.381	2.532	0.971
Chemotherapy	0.884	0.415	1.883	0.749
MYO1B	1.218	1.054	1.407	0.008

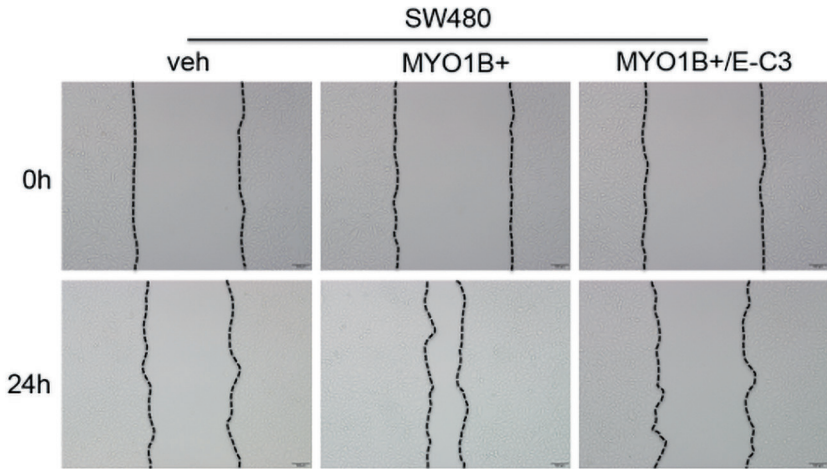

Figure S1 Representative figures for would healing assay.

https://dx.doi.org/10.21037/atm-21-4702